JPn Neuroscience
The Journal of Physiology

In vivo cholinergic modulation of the cellular properties of medial entorhinal cortex neurons

Yusuke Tsuno, Nathan W. Schultheiss and Michael E. Hasselmo

Center for Memory and Brain, Department of Psychology and Graduate Program for Neuroscience, Boston University, Boston, MA 02215, USA

Key points

- Medial entorhinal cortex neurons show special intrinsic properties *in vitro*, which might be important for contributing to functional cell properties, such as grid cell firing.
- Both intrinsic properties in slices of medial entorhinal cortex and grid cell activity *in vivo* are affected by cholinergic activation, but the relationships between these effects are unknown.
- Using intracellular recording, we show that intrinsic properties including sag amplitude, sag time constant and resonance frequency are affected by cholinergic activation *in vivo*, and these results are consistent with *in vitro* studies.
- Furthermore, we show that the relationship between firing frequency and input current is also changed by cholinergic activation in our *in vivo* recordings.
- These results suggest the importance of cholinergic influences on the intrinsic properties of medial entorhinal neurons, and help us understand how this influence contributes to mechanisms of spatial memory and the cause of memory impairment.

Abstract Extensive *in vitro* data and modeling studies suggest that intrinsic properties of medial entorhinal cortex (MEC) neurons contribute to the spiking behaviour of functional cell types of MEC neurons, such as grid cells, recorded in behaving animals. It remains unclear, however, how intrinsic properties of MEC neurons influence cellular dynamics in intact networks *in vivo*. In order to begin to bridge the gap between electrophysiological data sets from brain slices and behaving animals, in the present study we performed intracellular recordings using sharp electrodes in urethane-anaesthetized rats to elucidate the cellular dynamics of MEC neurons *in vivo*. We focused on the h-current-dependent sag potential during hyperpolarizing current steps, subthreshold resonance in response to oscillatory frequency sweeps (chirp stimuli), persistent spiking in response to brief depolarizing inputs and the relationship between firing frequency and input (*f–I* curve), each of which is sensitive to cholinergic modulation *in vitro*. Consistent with data from *in vitro* studies, cholinergic activation by systemic application of the acetylcholinesterase inhibitor, physostigmine, resulted in decreased sag amplitude, increased sag time constant and a decrease of the peak resonance frequency. The *f–I* curve was also modulated by physostigmine in many neurons, but persistent spiking was not observed in any of our recordings, even when picrotoxin, a $GABA_A$ blocker, was included in the internal solution of the recording pipette to reduce possible effects of network inhibition. These results suggest that intrinsic oscillatory and rate-coding mechanisms, but not intrinsic bistability, are significantly modulated by acetylcholine in the intact entorhinal network.

(Received 20 December 2012; accepted after revision 22 March 2013; first published online 25 March 2013)
Corresponding author Y. Tsuno: Center for Memory and Brain, Department of Psychology and Graduate Program for Neuroscience, Boston University, 2 Cummington Mall, Boston, MA 02215, USA. Email: ytsuno@bu.edu

DOI: 10.1113/jphysiol.2012.250431

Abbreviations AHP, after-hyperpolarization; Ctrl, control; EC, entorhinal cortex; FFT, fast Fourier transform; *f–I* curve, frequency–current curve; kg bwt, kilograms body weight; I_{CAN}, non-specific calcium-sensitive cationic current; I_h, hyperpolarization-activated cation current; MEC, medial entorhinal cortex; Phys, physostigmine; PTX, picrotoxin; R_{in}, input resistance; TRPC, transient receptor potential canonical.

Introduction

The medial entorhinal cortex (MEC) acts as the gateway for information flowing into and out of the hippocampus (Witter *et al.* 1989; van Strien *et al.* 2009). The MEC plays an important role in episodic memory, based on impairments of memory caused by lesions of the entorhinal cortex (EC) in rats (Steffenach *et al.* 2005) and primates (Leonard *et al.* 1995). Numerous extracellular recordings from EC in awake, behaving animals (Hafting *et al.* 2005; Newman *et al.* 2012) have identified distinct functional cell types, such as grid cells and head direction cells, that respond to environmental or behavioural parameters (Hafting *et al.* 2005; Moser & Moser, 2008; Brandon *et al.* 2011; Koenig *et al.* 2011), and *in vitro* recordings using brain slice preparations of EC have characterized the cellular properties of different morphologically defined cell types, including stellate cells in layers II/III and pyramidal neurons (Klink & Alonso, 1997*b*; Egorov *et al.* 2002; Erchova *et al.* 2004; Giocomo *et al.* 2007; Nolan *et al.* 2007; Garden *et al.* 2008; Heys *et al.* 2010; Heys & Hasselmo, 2012). However, only a few previous studies have addressed the link between the dynamics of MEC neurons *in vitro* and *in vivo* (Quilichini *et al.* 2010; Hahn *et al.* 2012; Domnisoru *et al.* 2013; Schmidt-Hieber & Häusser, 2013). In the present study, we focused on layer II/III cells in MEC and performed intracellular recordings in urethane-anaesthetized rats to characterize cellular properties *in vivo* that have been proposed, based on *in vitro* studies, to contribute to neural function in behaving animals.

Acetylcholine is critical for performance in memory tasks (for review see Hasselmo, 2006; Heys *et al.* 2012; Newman *et al.* 2012) and modulates many of the neurophysiological properties in EC thought to underlie spatial processing (Klink & Alonso, 1997*b*; Egorov *et al.* 2002; Heys *et al.* 2010). Neurons in MEC exhibit subthreshold resonance (Erchova *et al.* 2004; Giocomo *et al.* 2007; Hu *et al.* 2009; Heys *et al.* 2010) in the theta frequency range (4–12 Hz), reflecting bandpass filtering (Hutcheon & Yarom, 2000) imparted by cellular properties including the hyperpolarization-activated cation current, I_h (Dickson *et al.* 2000; Heys *et al.* 2010; Heys & Hasselmo, 2012). We delivered hyperpolarizing current steps and sweeps of increasing frequency stimulation (chirps) before and after systemic administration of the acetylcholinesterase inhibitor, physostigmine, to test *in vivo* the robustness of h-current activation and whether resonance frequency decreases during cholinergic activation as it does *in vitro* (Heys *et al.* 2010).

Persistent spiking is defined here as a phenomenon of sustained spiking that can be elicited from quiescence by a brief depolarizing input (Klink & Alonso, 1997*b*; Egorov *et al.* 2002; Fransén *et al.* 2006; Heys *et al.* 2012). This phenomenon is also dependent on cholinergic modulation *in vitro* and has been proposed as a cellular substrate for working memory encoding (Schon *et al.* 2004, 2005; Hasselmo & Stern, 2006). We delivered strong, transient current steps to drive high spike rates briefly in our recorded neurons and assessed spiking after the input for evidence of self-sustained spiking or persistently elevated spike rates. Finally, we also used slow, linearly increasing ramp stimuli to test the relationship of spike frequency response to current input and to determine *in vivo* how cholinergic modulation might affect the gain of input–output relationships for MEC neurons.

Methods

Animal surgery

Experiments were performed on 30 adult male Long–Evans rats (250–400 g; Charles River Laboratories, Wilmington, MA, USA), from which 14 successful neuronal recordings were used for analysis. An additional eight rats were used for six successful neuronal recordings for saline control experiments. Animals were anaesthetized with an intraperitoneal injection of urethane (1.2–1.5 g (kg bwt)$^{-1}$), and additional doses of urethane were given as needed (0.3–0.4 g (kg bwt)$^{-1}$). Body temperature was maintained with a disposable heating pad. The depth of anaesthesia and the rhythm of breathing were monitored during the entire experiment. Before surgery, bupivacaine was injected subcutaneously at the site of the incision, and an injection cannula was placed intraperitoneally to allow drug administration during the experiment. Each rat was placed in a stereotaxic apparatus (SR-8N; Narishige, Setagaya-ku, Tokyo, Japan) and prepared for acute electrophysiological recording from the MEC. Two holes were drilled for the hippocampus (posterior 4.2 mm, lateral 3.0 mm from bregma) and MEC (lateral 4.5 mm from lambda and the intersection with the lambdoidal suture). For recording the hippocampal EEG, twisted Teflon-insulated stainless-steel electrodes (#790900; A-M Systems, Sequim, WA, USA) were implanted in the stratum radiatum of the dorsal CA1 hippocampus (posterior 4.2 mm, lateral 3.0 mm from bregma; depth 2.4 mm from the surface) and secured in place using dental cement. Agarose was

put on the surface of the brain above the MEC to reduce pulsation, drying and instability. An Ag–AgCl pellet was placed in the neck muscles as a reference electrode for intracellular recording.

Ethical approval

All experiments were performed in accordance with experimental guidelines approved by the Institutional Animal Care and Use Committee at Boston University and The Animal Welfare Act.

Electrophysiology

Intracellular recordings were performed with sharp intracellular recording electrodes created from glass capillaries (#BF150-86-10; Sutter Instruments, Novato, CA, USA) on an electrode puller (P-87 or P-97; Sutter Instruments). The internal solution for the micropipette electrode included 2 M potassium acetate, 2% biotin dextran amine (Dextran, Biotin, 3000 MW, Lysine Fixable, BDA-3000, #D-7135; Life Technologies, Grand Island, NY, USA) or 2% neurobiotin (#SP-1120; Vector Laboratories, Burlingame, CA, USA) or 2% biocytin (#B4261; Sigma, St. Louis, MO, USA). Micropipette impedance was 40–70 MΩ. The electrode was lowered to the MEC (lateral 4.5 mm, 0.35–1.00 mm anterior from the sinus on the cerebellum, angled 12 degrees to anterior, depth 2.0–4.5 mm from the surface) by a micromanipulator (MO-8-W; Narishige). An electronic buzz was performed to make the micropipette penetrate the cell membrane. The intracellular membrane potential and hippocampal EEG signal were amplified (Multiclamp 700B; Molecular Devices, Sunnyvale, CA, USA) and stored in a computer via an analog-to-digital (A/D) converter (Digidata 1440A; Molecular Devices) with pCLAMP software (sampling rates 10 kHz). Mechanical noise was reduced by use of an air table, and an audio monitor and oscilloscope were used to assist in searching for cells. In some experiments, the internal solution of the recording micropipette included 1 mM picrotoxin (#1128; Tocris, Bristol, England, UK) diluted in DMSO. In order to allow the picrotoxin to diffuse fully within the recorded cell, we waited 30 min after the initiation of intracellular recording (Yazaki-Sugiyama *et al.* 2009) before gathering data on persistent spiking in these conditions. During recording, the acetylcholinesterase inhibitor, physostigmine (0.4 mg (kg bwt)$^{-1}$, #E8375 Eserine; Sigma), was administered intraperitoneally via the injection cannula. Although this is a systemic injection, it will increase the response to the endogenous local release of acetylcholine. In some cases, scopolamine methylbromide (0.1 mg (kg bwt)$^{-1}$; Sigma), which does not cross the blood–brain barrier, was injected intraperitoneally beforehand to prevent excessive salivation caused by physostigmine administration. Only recordings with resting membrane potentials more hyperpolarized than −60 mV and spike peaks higher than −20 mV were used for analysis. All spike amplitudes were greater than 55 mV. At the end of each recording, current pulses were applied for biotin labelling (±1–2 nA, 500 ms at 1 Hz for 10–25 min).

Histology

After the completion of each experiment, the depth of anaesthesia was increased with an intraperitoneal injection of urethane (0.3 − 1.5 g (kg bwt)$^{-1}$), and the animals were perfused with saline and 10% formalin transcardially. The brains were removed and postfixed overnight, and then put into 30% sucrose for cryoprotection. The brains were sliced into 50- or 100-μm-thick parasagittal sections using a cryostat (Leica, Buffalo Grove, IL, USA). Biotin-loaded cells were visualized using avidin–biotin complex [Vectastain Elite ABC kit (Standard), #PK-6100; Vector Laboratories] and DAB reactions (DAB Peroxidase Substrate Kit, #SK-4100; Vector Laboratories). The sections were mounted on gelatin-coated slides and counterstained with Neutral Red or Cresyl Violet.

Data analysis

Under urethane anaesthesia, there are two brain states, a fast-wave state (prominent 2–4 Hz) and a slow-wave state (prominent 0.5–1 Hz), which can be distinguished by EEG (Murakami *et al.* 2005; Wolansky *et al.* 2006; Tsuno *et al.* 2008; Schall & Dickson, 2010). Cholinergic neurons are active in the fast-wave state (Manns *et al.* 2000). In this experiment, we used a relatively high dose of urethane to maintain a deeply anaesthetized slow-wave state to ensure that the cholinergic system was not active before drug (physostigmine) injection. Physostigmine was then used to increase the levels of acetylcholine in the brain. All statistical comparisons were made with Student's two-tailed *t* tests.

Power spectra of hippocampal EEG. Power spectra were calculated from the downsampled hippocampal EEG (1 kHz) during a 50 s period from 60 s before and 15 min after physostigmine administration. The resolution of the power spectra was 0.122 Hz. The calculation was performed by pCLAMP.

Sag analysis. As a result of the rectifying nature of I_h, its time course and amplitude could be measured by applying hyperpolarizing current steps (−1000 pA for 2 s) and analysing the resulting 'sag' in the membrane potential back towards resting potential (Alonso & Klink, 1993; Giocomo & Hasselmo, 2008). Hyperpolarizing

current steps were initiated from a membrane potential of approximately −70 mV, which was achieved, when necessary, using tonic applied current. We measured the sag potential amplitude as the difference between the peak hyperpolarization elicited by negative current steps and the steady-state voltage during the 2 s stimulus. In order to minimize variability in sag measurements across cells resulting from differences in input resistance, we normalized the raw sag potential amplitude by the peak hyperpolarization elicited by the stimulus. Only neurons which showed a raw sag potential larger than 3 mV were tested for cholinergic effects on sag potential. The membrane potential during the sag was fitted to a single exponential function instead of a double exponential, because the slow component of sag was not clear *in vivo* and the single exponential was better for fitting. The amplitude and time constant of the sag were calculated using the Clampfit utility of pCLAMP software.

Analysis of subthreshold resonance. Chirp stimuli (frequency sweeps) consisted of a constant-amplitude (100 or 200 pA) sinusoidal current, which increased in frequency linearly from 0 to 50 Hz over a 50 s period (Giocomo *et al.* 2007; Heys *et al.* 2010). These stimuli were generated with the MATLAB chirp function and used to obtain the impedance amplitude profile of recorded neurons. In order to maintain the membrane potential of each cell low enough to prevent spiking during chirp stimulation (between –69 and –77 mV), a steady hyperpolarizing current was injected when necessary (between 0 and –500 pA). Only the data for which the difference of the membrane potential during current injection was less than 3 mV were used for comparison between control and physostigmine conditions. During the frequency sweep, the resulting voltage response, $V(t)$, was measured, and the frequency-dependent impedance profile, $Z(f)$, was calculated by taking the fast Fourier transform (FFT) of the membrane potential with chirp stimulation $[V_f(t)]$ minus the FFT of the membrane potential without chirp stimulation $[V_{control,f}(t)]$, and the difference between these values was divided by the FFT of the injected sinusoidal current $[I_f(t)]$. Subtraction was performed to reduce the effect of *in vivo* oscillatory dynamics, such as network slow-wave oscillations, which are independent from the chirp stimulation, as follows:

$$Z(f) = \frac{FFT[V_f(t)] - FFT[V_{control,f}(t)]}{FFT[I_f(t)]}$$

The resonance frequency, f_{res}, was defined as the stimulus frequency that maximized $Z(f)$. Fitting for $Z(f)$ was done using a 10th-order polynomial, and the resonance frequency, f_{res}, was detected as the peak of the fitting. Cholinergic modulation of resonance frequency was tested for those cells that showed a clear peak in resonance frequency.

Spike frequency during injected ramp current (*f–I* curve). In order to analyse the frequency–current (*f–I*) relationship of each cell with a single stimulus application, we delivered slow, linearly increasing and decreasing current ramps, starting from a tonic current injection level that held each cell below the threshold for tonic spiking. Ramp stimuli have been used previously in studies of motoneurons, wherein hysteresis was categorized as type 1–4 (Button *et al.* 2006) or clockwise/counterclockwise (Iglesias *et al.* 2011). We used this framework to characterize the spiking responses of MEC neurons to ramp stimuli and to test the effects of cholinergic modulation on intrinsic properties in MEC neurons. A 45 s upward ramp (increasing to 1000 pA) followed by a 45 s downward ramp current stimulation was used. After each ramp stimulation, a negative current pulse (–1000 pA for 2 s) was applied to eliminate potential effects of the ramp stimulus on persistent spiking. After detection of all of the spikes during the stimulus, instantaneous frequencies of spiking were calculated from the interspike intervals. The *f–I* curve was obtained for each recorded neuron by smoothing instantaneous spike frequencies during ramp stimulation with a sliding window spanning 10 spike cycles and then anchoring to the respective instantaneous injected current values. The initial up-ramp slope, terminal up-ramp slope, initial down-ramp slope and terminal down-ramp slope of the *f–I* curve were measured with linear fitting to segments of the *f–I* curve containing at least 20 interspike intervals during at least 10 s of stimulation. This approach allowed reasonable estimates of the *f–I* curve slope despite local variations in spike rate caused by slow-wave activity. The averaged slopes were calculated across one to four stimulus repetitions for each condition. Analysis was done using MATLAB. Spike threshold was determined for the first spike during up-ramp stimulation and the last spike during down-ramp stimulation. Thresholds of spikes were determined by the highest slope of the change of the membrane potential immediately before the action potentials. Average values across one to five stimuli were used for analysis. If spikes occurred before up-ramp stimulation or after down-ramp stimulation, the spike threshold was not determined.

Results

Effects of physostigmine confirmed by the change of hippocampal EEG

We used systemic injections of physostigmine, an acetylcholinesterase inhibitor, to enhance cholinergic modulation during the experiments. In our recordings,

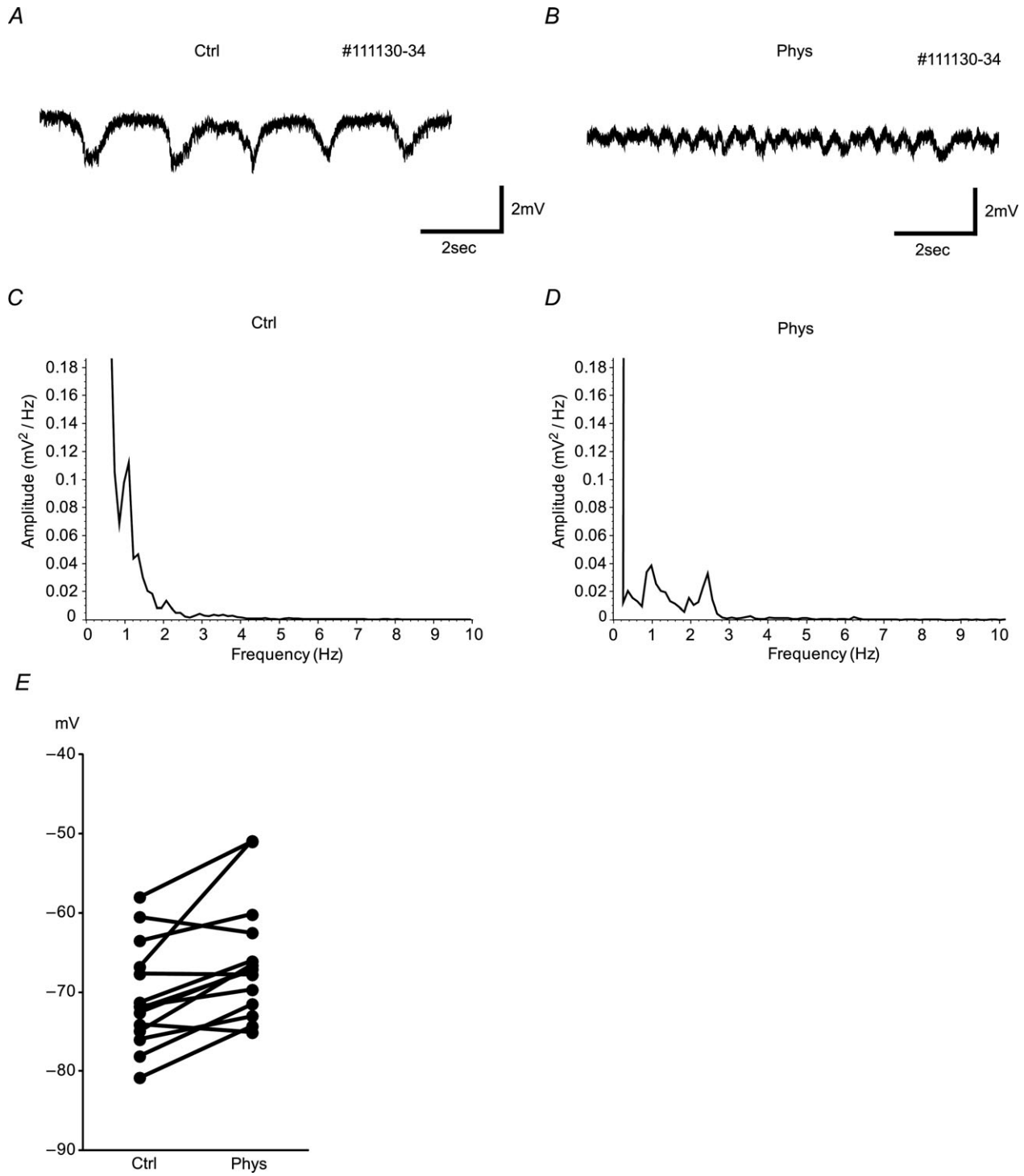

Figure 1. Hippocampal EEG and membrane potentials change after physostigmine (Phys) application
A and *B*, examples of hippocampal EEG are shown 30 s before (*A*) and 15 min after the physostigmine application intraperitoneally (*B*). Hippocampal EEG changed from a 0.5–1 Hz slow oscillation to a 2–4 Hz faster oscillation. *C* and *D*, power spectra of the hippocampal EEG in control condition (*C*) and in the presence of physostigmine (*D*). Relatively large power is observed in the 0.5–1 Hz band in control conditions (*C*) and in the 2–4 Hz band in the presence of physostigmine (*D*). *E*, averages of membrane potentials before (Ctrl) and after physostigmine application with no current injection. Ten of 14 cells showed a significant increase of membrane potentials. Averages were −70.6 (Ctrl) and −65.9 mV (Phys).

the hippocampal EEG, which is highly modulated by cholinergic input, transitioned from a slow-wave pattern during the deeply anaesthetized state before physostigmine application (Fig. 1*A* and *C*), to a fast-wave pattern (Fig. 1*B* and *D*) after physostigmine application. By observing the change of hippocampal EEG from slow wave to fast wave, we confirmed that physostigmine application was effective in increasing cholinergic modulation.

Change of membrane potential after physostigmine application

We analysed the data to see whether physostigmine application changed the membrane potential of the recorded cells ($n = 14$; Fig. 1*E*). Ten of 14 neurons showed a significant increase of membrane potential ($P < 0.001$, Student's two-tailed unpaired *t* test). Averages of membrane potentials of cells were -70.6 ± 1.69 mV (mean ± SEM) in the control conditions and -65.9 ± 1.96 mV in the physostigmine conditions with no current injection (14 cells, $P < 0.01$, Student's two-tailed paired *t* test). The value of resting membrane potential in the control conditions is consistent with a previous report (Quilichini *et al.* 2010). For the experiment on sag potentials and resonance frequency, if the membrane potential changed after physostigmine application, the membrane potentials were matched between the two conditions by using current injection. If the membrane potentials differed by more than 7 mV between the two conditions, the data were eliminated.

Cholinergic modulation of h-current *in vivo*

We focused on recordings from neurons in MEC layers II (Klink & Alonso, 1997*a*; Quilichini *et al.* 2010) and III (Dickson *et al.* 1997; Gloveli *et al.* 1997; Quilichini *et al.* 2010) as verified with histological staining (Fig. 2) to elucidate the effects of cholinergic modulation on cellular physiology *in vivo*. Of the 14 cells recorded

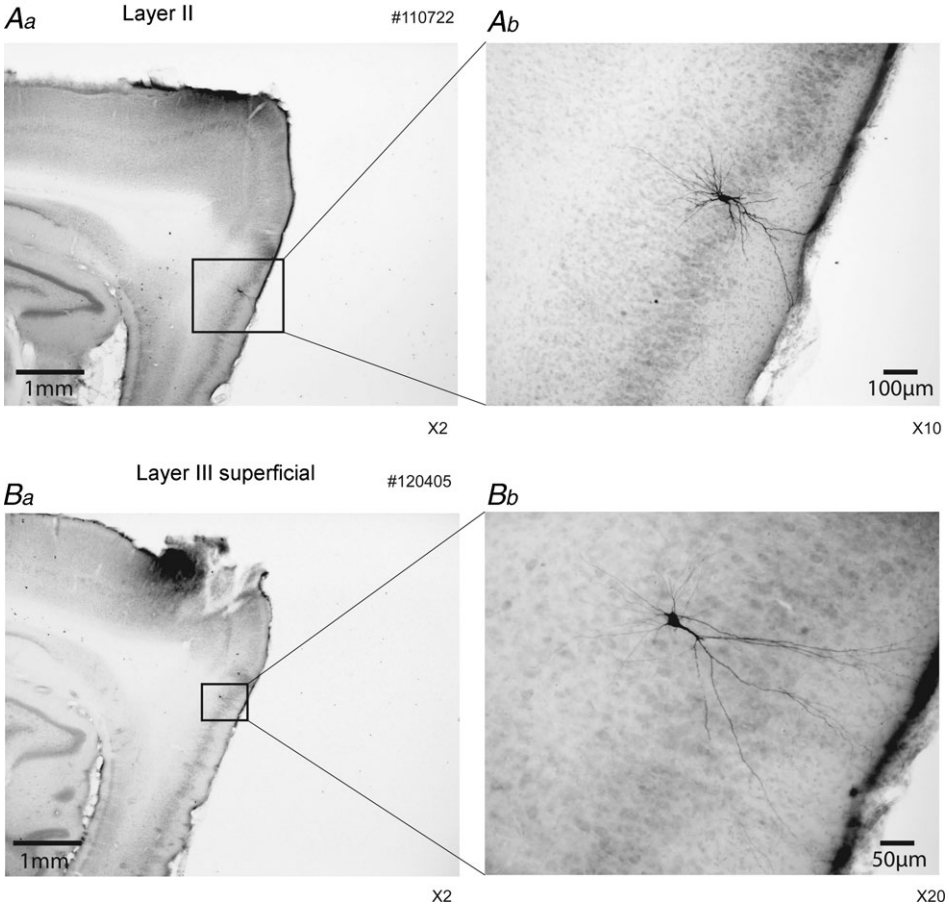

Figure 2. Examples of the recorded cells
Aa, layer II cell (parasagittal section). *Ab*, higher magnification of *Aa*. The biotin-labelled cell is a stellate cell in layer II of the medial entorhinal cortex (MEC). *Ba*, layer III superficial cell (parasagittal section). *Bb*, higher magnification of *Ba*. This neuron shows non-spiny dendrites, and the initial bifurcation is close to the cell body, which indicates a type 2 projection neuron as described by Gloveli *et al.* (1997).

in this study, 11 cells were putative stellate cells in layer II, two cells were in layer III, and one cell was in layer II or III. Stellate cells of layer II/III of the MEC possess a strong hyperpolarization-activated, mixed cation current (h-current) mediated by HCN channels (Ludwig *et al.* 1998; Dickson *et al.* 2000). The h-current is inwardly rectifying and underlies the prominent sag potential exhibited by entorhinal stellate cells, which consists of a slower depolarization of the membrane potential during negative applied current steps after the initial hyperpolarization at the onset of the stimulus. We applied 2 s current steps of −1000 pA to characterize the sag potential and input resistance of layer II/III MEC neurons *in vivo* in conditions with and without

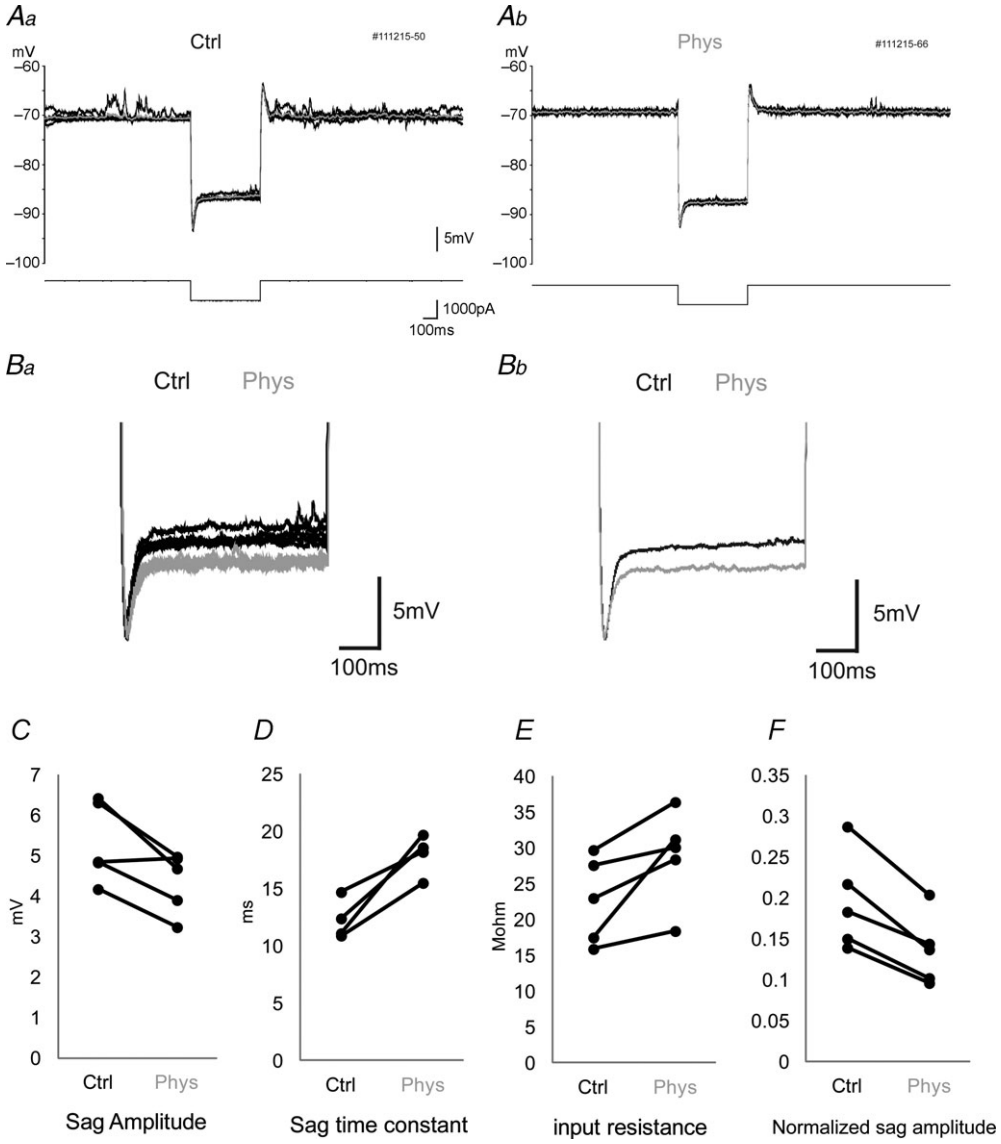

Figure 3. Sag potential amplitude and time constant during physostigmine application
A, membrane potential response (upper traces) to current square pulse (−1000 pA) stimulation (lower traces) in control conditions (*A*a) and after physostigmine application (*A*b). A large sag potential is observed immediately after the initiation of the current pulse. Five traces are overlaid, and the grey trace is the average. *B*, higher magnification of sag potentials. Five raw traces (*B*a) and averaged traces (*B*b) are overlaid in control conditions (black) and after physostigmine application (grey). Traces were aligned with the trough immediately after the onset of negative current stimulation. *C*–*F*, averaged values of sag amplitude (*C*), sag time constant (*D*), input resistance (*E*) and normalized sag amplitude (*F*) in individual neurons in control conditions (Ctrl) and in the presence of physostigmine (Phys). Each connected pair indicates the data from a single cell. The normalized sag amplitude (*F*) is calculated as sag amplitude divided by the amplitude of the initial negative potential immediately after the negative current pulse to cancel out the effect of input resistance change on sag amplitude. There is a significant increase in the sag time constant during physostigmine application.

increased cholinergic modulation due to physostigmine administration (Fig. 3*A* and *B*). With physostigmine, the sag potential amplitude decreased significantly from 5.32 ± 0.45 to 4.34 ± 0.34 mV (mean ± SEM; Fig. 3*C*; $P < 0.05$, Student's two-tailed paired *t* test, $n = 5$). The time constant of the sag showed an increase from 12.3 ± 0.9 to 18.0 ± 0.9 ms (Fig. 3*D*; $P < 0.05$, $n = 4$), and input resistance increased from 22.7 ± 2.7 to 28.9 ± 3.0 MΩ (Fig. 3*E*; $P < 0.05$, $n = 5$). The normalized amplitude of the sag potential was reduced significantly from 0.20 ± 0.03 to 0.14 ± 0.02 (Fig. 3*F*; $P < 0.01$, $n = 5$). These data *in vivo* replicate the effects of bath application of the acetylcholine receptor agonist, carbachol, in brain slice preparations (Heys *et al.* 2010). None of these changes was observed after intraperitoneal injection of saline instead of physostigmine ($P > 0.05$, $n = 5$).

Cholinergic modulation of subthreshold resonance *in vivo*

Subthreshold resonance is a reflection of the preferential responsiveness that a neuron may possess to inputs with particular frequency composition. Stellate cells in the MEC exhibit subthreshold resonance in the theta frequency range as a consequence, in part, of the time constants of h-current activation, which acts as a high-pass filter by opposing slow changes in voltage by inward rectification. It was recently reported that cholinergic modulation with carbachol reduces the peak resonance frequency of MEC stellate cells recorded *in vitro* during stimulation with frequency sweeps of sinusoidal current, referred to as chirp or ZAP stimuli (Heys *et al.* 2010). Heys and colleagues also reported that co-administration of carbachol and the selective h-current blocker, ZD7288, yielded no additional effect on the impedance profile and sag potential of MEC stellate cells, suggesting that the effect on subthreshold resonance is also mediated by the modulation of h-current. During our intracellular recordings, we applied chirp stimuli composed of linearly increasing frequencies (from 0 to 50 Hz) of sinusoidal current injection and derived the impedance profiles of MEC neurons *in vivo*, taking the peak of the impedance profile as the resonance frequency (Fig. 4*A*–*D*). The average resonance frequency was significantly reduced from 11.4 ± 0.9 to 8.7 ± 1.1 Hz (mean ± SEM) after physostigmine application (Fig. 4*E*; $P < 0.05$, Student's two-tailed paired *t* test, $n = 4$), confirming *in vivo* the reduction of resonance frequency by cholinergic modulation observed *in vitro* (Heys *et al.* 2010). No significant reduction of resonance frequency was observed in experiments in which a saline injection was administered instead of physostigmine ($P > 0.05$, $n = 5$).

Absence of bistable persistent spiking *in vivo*

Bistable persistent spiking in the MEC entails a self-sustained spiking state mediated by a non-specific calcium-sensitive cationic current (I_{CAN}; Fransén *et al.* 2006) via TRPC channels (Zhang *et al.* 2011), which can be elicited *in vitro* from quiescence with a brief depolarizing current step. Bistable persistent spiking has been proposed to underlie the elevated spiking observed in EC of behaving monkeys and rats during the delay period of delayed match to sample tasks (Suzuki *et al.* 1997; Young *et al.* 1997), and therefore as a cellular substrate for information held in working memory (Camperi & Wang, 1998). However, there is no experimental evidence to date that distinguishes whether bistable persistent spiking and/or network mechanisms, such as recurrent excitation (Major & Tank, 2004), underlie delay activity in behaving animals.

In order to examine whether bistable persistent spiking is robust in the intact entorhinal network *in vivo*, during our intracellular recordings we delivered positive current pulses to MEC neurons before and after physostigmine application (Fig. 5), mimicking as closely as possible the *in vitro* protocols for eliciting bistable persistent spiking with cholinergic modulation (Egorov *et al.* 2002; Tahvildari *et al.* 2007; Schultheiss & Hasselmo, 2011). We started the protocol by changing the basal injection current amplitude to set the membrane potential slightly below the spike threshold, and we then presented a positive current pulse (1000 pA for 2 s) to drive spiking briefly at a high rate. Spiking subsequent to the current pulse was analysed to determine whether a persistent spiking state was elicited by the inputs or whether there was a consistent effect on mean spike frequency. Contrary to expectations, persistent spiking could not be elicited during cholinergic activation in any of our recordings (Fig. 5*A*b, *B*b and *B*c), and there was no consistent effect of current pulse stimuli on the subsequent spike rate; seven of nine neurons showed no effect whatsoever. Although the remaining two neurons showed a slight increase in spiking after the first current pulse delivered following physostigmine administration, this change could not be elicited consistently, and firing frequency was not reduced by delivery of a subsequent negative current pulse as expected based on *in vitro* studies (Egorov *et al.* 2002; Tahvildari *et al.* 2007). In an additional two experiments, the $GABA_A$ receptor antagonist, picrotoxin, was included in the recording micropipette to block inhibitory input to the recorded neurons selectively. These two neurons showed a slight increase of firing frequency after one current pulse, but this also did not occur consistently (Fig. 5*B*a–c). In both cases, we were unable to elicit persistent spiking even in the absence of synaptic inhibition.

Slope of spike frequency to input current (*f–I* curve) increased by cholinergic modulation

In order to characterize the effect of cholinergic modulation on the relationship of firing frequency to injected current, we delivered slow, linearly increasing and decreasing current ramp stimuli (up- and down-ramps) before and after physostigmine application (Fig. 6). Recordings showed that firing frequency increased during up-ramp stimulation and decreased during down-ramp stimulation. Quantitative analysis showed that the initial up-ramp slope of the *f–I* curve became steeper after physostigmine application than the slope observed before physostigmine application ($P < 0.05$, Student's two-tailed paired t test, $n = 10$), suggesting that the sensitivity to input increased during cholinergic modulation. For five

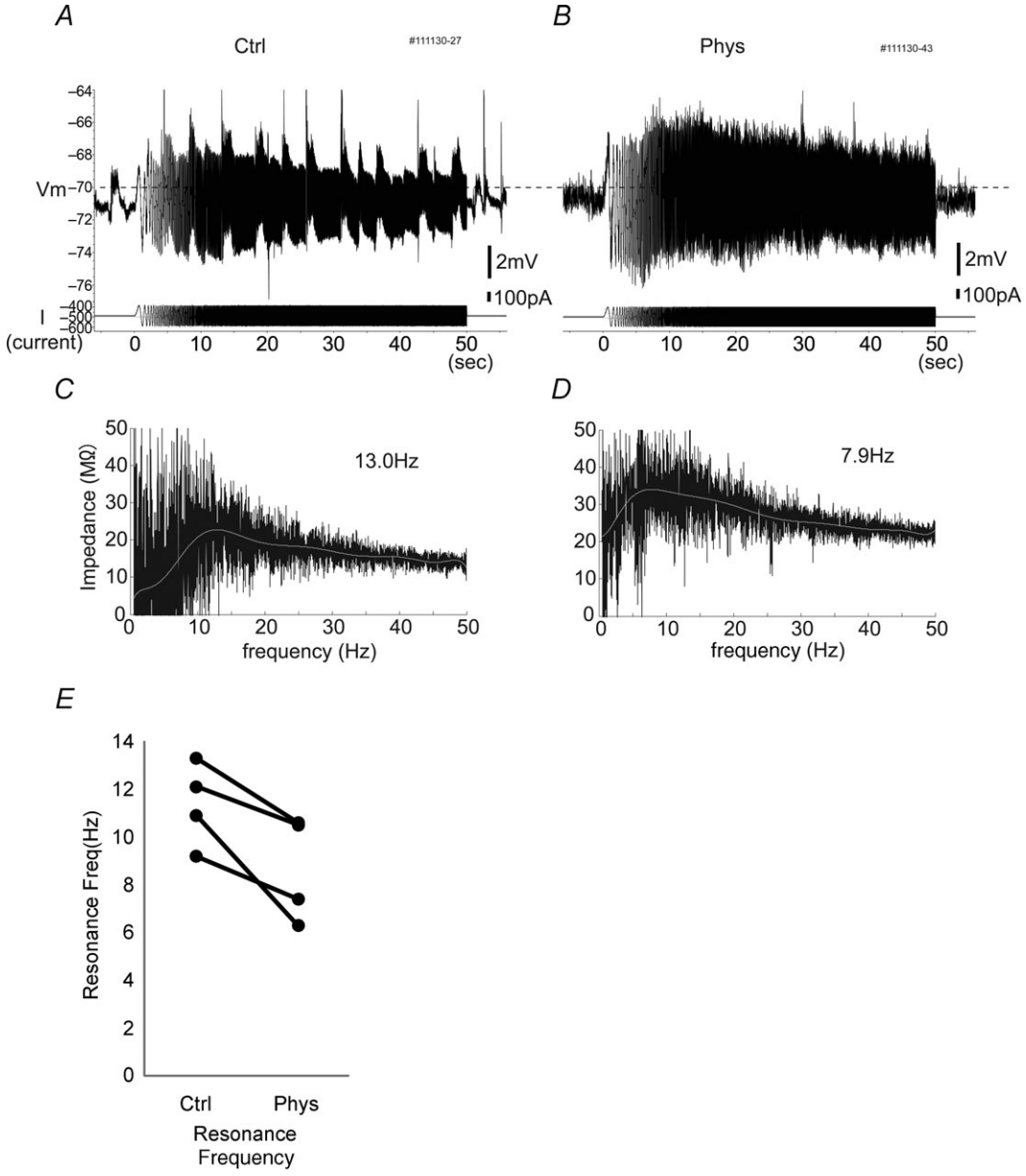

Figure 4. Resonance frequency becomes lower after physostigmine application
A and *B*, raw traces of the response to frequency sweep (chirp) stimulation in control conditions (*A*) and in the presence of physostigmine (*B*). Top traces are membrane potential; bottom traces are injected current. Chirp stimulation consists of a sine wave that increases in frequency from 0 to 50 Hz linearly over 50 s. The dashed line indicates −70 mV. *C* and *D*, impedance profile in each frequency calculated by the response amplitude (*A* and *B*) of chirp stimulation in control conditions (*C*) and in the presence of physostigmine (*D*). Grey trace indicates the fitted trace using a 10th-order polynomial. Note that the resonance (peak) frequency shifted from 13.0 to 7.9 Hz after physostigmine administration. *E*, averaged values of resonance frequencies in individual neurons ($n = 4$, $P < 0.05$).

of 10 neurons, the average slope of the initial up-ramp *f–I* curve became more than 2.0 times steeper after physostigmine injection than prior to physostigmine injection (Fig. 7*A*), and for three of the remaining neurons, the initial *f–I* slope was increased by 1.2–2.0 times (Fig. 7*B*). The final two neurons showed a ratio less than 1.2 (Fig. 7*C*). Thus, five neurons showed large modulation and three neurons showed moderate modulation by

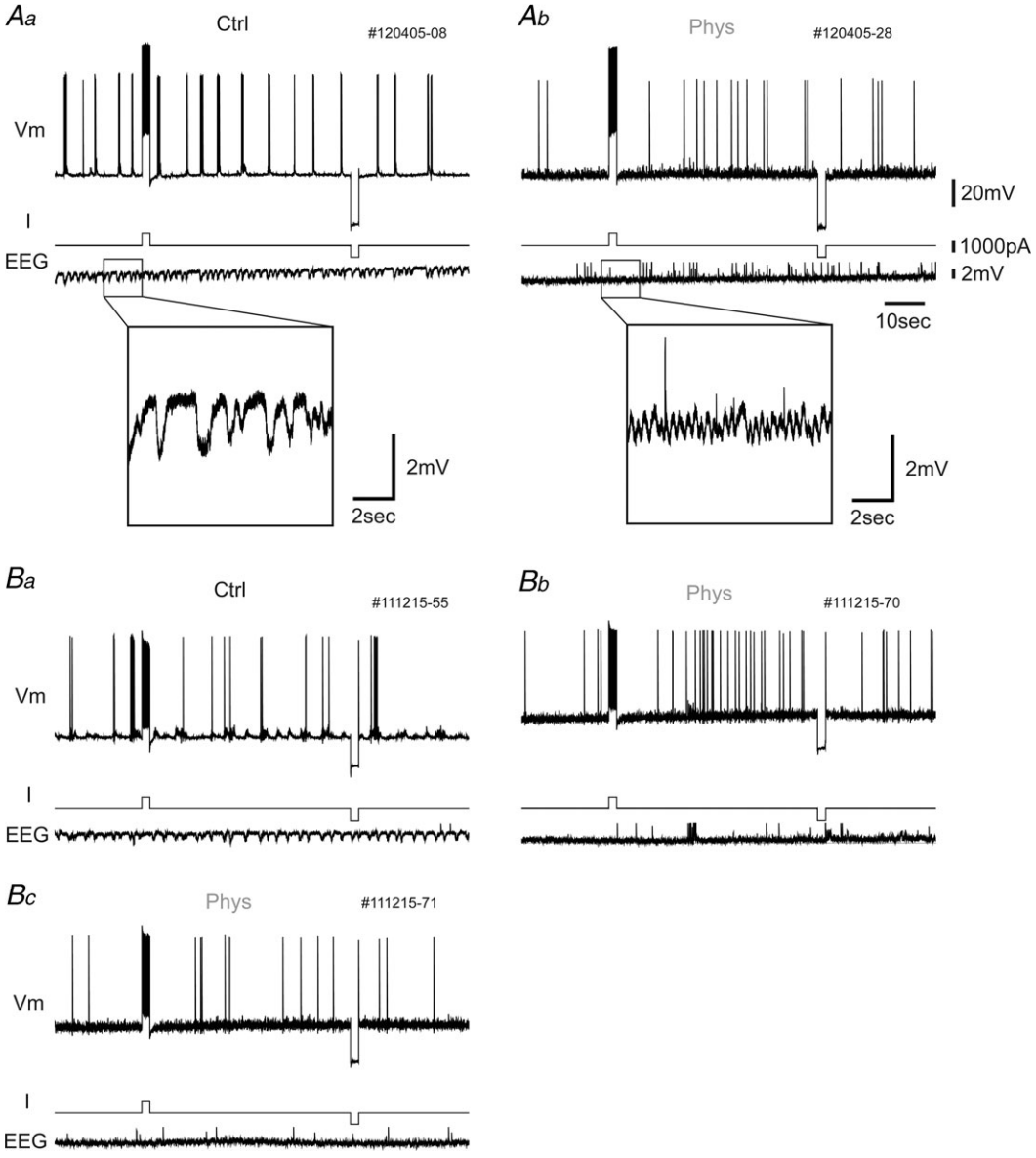

Figure 5. Persistent spiking did not appear *in vivo* under urethane anaesthesia
A, one example of the response to current pulse injection. Top traces, membrane potential (V_m); middle traces, injected current (*I*); and bottom traces, hippocampal EEG (EEG). *Aa*, in this protocol, membrane potential is first set slightly below the level of constant spike firing by changing the injected current. Then, a 1000 pA, 2 s current pulse is injected to elicit persistent firing after the cessation of current stimulation. After the waiting period (50 s), a 2 s negative current pulse (−1000 pA) is injected to eliminate any remaining effect of the positive current pulse. The hippocampal EEG shows slow-wave activity in the control condition (inset, higher magnification). *Ab*, in the presence of physostigmine, persistent spiking does not occur after current pulse injection. The hippocampal EEG shows fast-wave activity due to physostigmine administration (inset, higher magnification). *B*, another example of the response to current pulse injection with picrotoxin in the recording pipette. *Ba*, there is no change of spiking in control condition. *Bb*, after physostigmine application, the cell tends to increase firing rate after the positive current pulse in this case, but does not show continuous persistent spiking. *Bc*, this is the response of the same neuron with the same current injection protocol as shown in *Bb*, but the neuron does not show an increase in firing frequency again.

physostigmine application of the initial slope during the up-ramp. Further analysis of the *in vivo f–I* curves showed that some neurons exhibited clockwise hysteresis (categorized as a type 2 *f–I* relationship by Button *et al.* 2006), i.e. firing frequency increased rapidly at first (large initial *f–I* slope), reaching a plateau frequency of approximately 15–25 Hz during the up-ramp (flat terminal slope), before subsequently decreasing with an intermediate slope during the down-ramp. As a measure of this hysteresis, we compared the initial down-ramp slope with the terminal up-ramp slope. Both in control conditions and in the presence of physostigmine, the average slope of the initial down-ramp was steeper than that of the terminal up-ramp ($P < 0.05$ and $P < 0.01$, respectively, Student's two-tailed paired t test, $n = 10$). In order to examine the change of the hysteresis property by physostigmine application, the ratio of the initial down-ramp slope to the last up-ramp slope was compared between control and physostigmine conditions. Two of 10 neurons showed that the ratio in the presence of physostigmine was more than 2 times larger than that in control conditions. Overall, however, there was no significant difference between the ratio in control conditions and in the presence of physostigmine ($P = 0.24$, Student's two-tailed paired t test, $n = 10$). In these experiments, persistent spiking was never observed after ramp stimulation, which differs from results in our *in vitro* studies (N. W. Schultheiss and M. E. Hasselmo, unpublished observations). All parameters of ramp stimulation data are summarized in Table 1.

Change of spike threshold by cholinergic modulation

We examined the threshold of the first spike during up-ramp stimulation and the threshold of the last spike during down-ramp stimulation. There were no

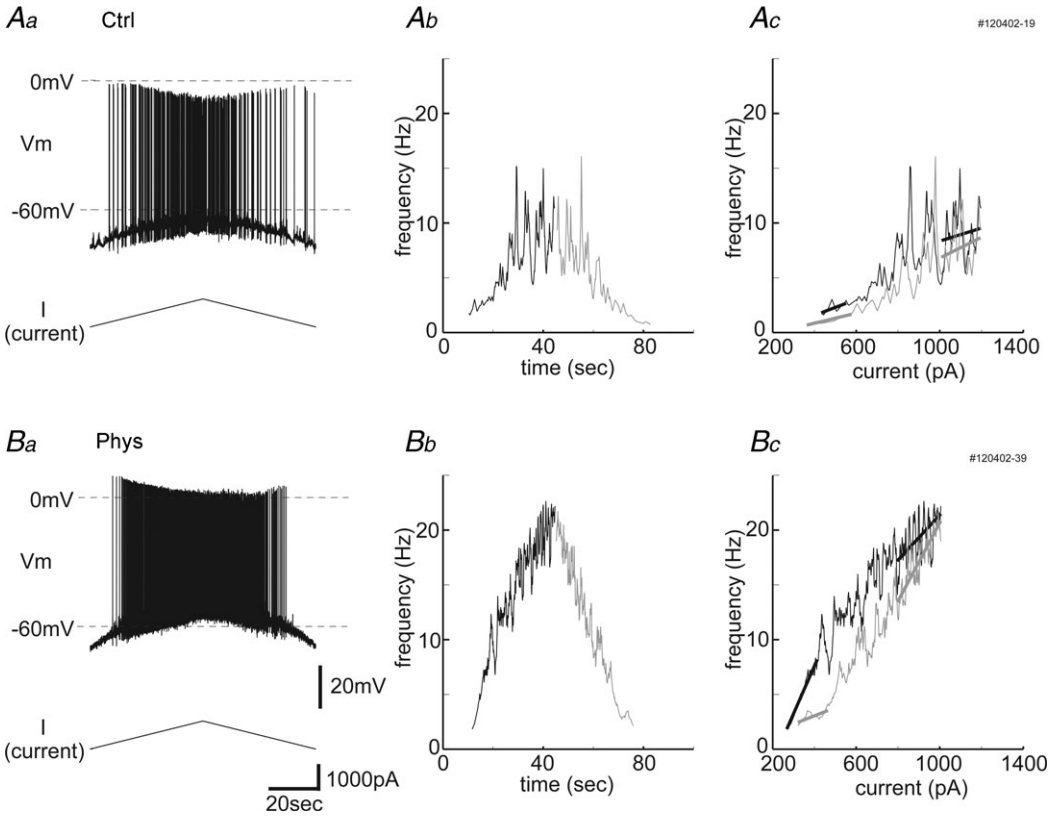

Figure 6. The frequency–current (*f–I*) curve becomes steeper after physostigmine application
Increasing and decreasing ramp stimulation (1000 pA) is used to examine the *f–I* curve properties in control conditions (*Aa–c*) and in the presence of physostigmine (*Ba–c*). *Aa* and *Ba*, top traces, membrane potential and bottom traces, injected current. *Ab* and *Bb*, the relationships between time and frequency of spikes. Black traces are during the up-ramp, and grey traces are during the down-ramp. The traces are smoothed by averaging 10 interspike intervals. *Ac* and *Bc*, *f–I* plot. Black traces are during the up-ramp, and grey traces are during the down-ramp. Initial up-ramp slope, terminal up-ramp slope (black lines), initial down-ramp slope and terminal down-ramp slope (grey lines) of the *f–I* curve were calculated by linear fitting. Note that the initial up-ramp slope in the presence of physostigmine (*Bc*) is steeper than that in control conditions (*Ac*). Recordings show a slight hysteresis, which means a steeper initial slope during the down-ramp than the terminal slope during the up-ramp. This was observed more prominently after physostigmine injection (*Bc*).

differences between the thresholds of the first spike during up-ramp and the thresholds of the last spike during the down-ramp either without or with physostigmine ($P = 0.94$ and $P = 0.36$, respectively, $n = 7$). However, spike threshold was increased after physostigmine administration relative to control conditions from -55.4 ± 2.3 to -48.0 ± 2.8 mV (mean ± SEM) for the first spike during the up-ramp (Fig. 8*A*; $P < 0.01$, Student's two-tailed paired *t* test, $n = 8$) and from -55.4 ± 2.6 to -49.0 ± 3.3 mV (Fig. 8*B*; $P < 0.05$, $n = 7$) for the last spiking during the down-ramp. No significant differences of spike threshold were observed in experiments in which a saline injection was administered instead of physostigmine ($P > 0.05$, respectively, $n = 4$).

Discussion

In the present study, we explored cellular properties of MEC neurons that have been proposed to contribute to the spatial function of entorhinal cortex. We show that acetylcholine activation *in vivo* modulates sag potentials, subthreshold resonance and the *f–I* curve, as it does *in vitro*, supporting interpretations of the contributions of these properties to MEC function in behaving animals.

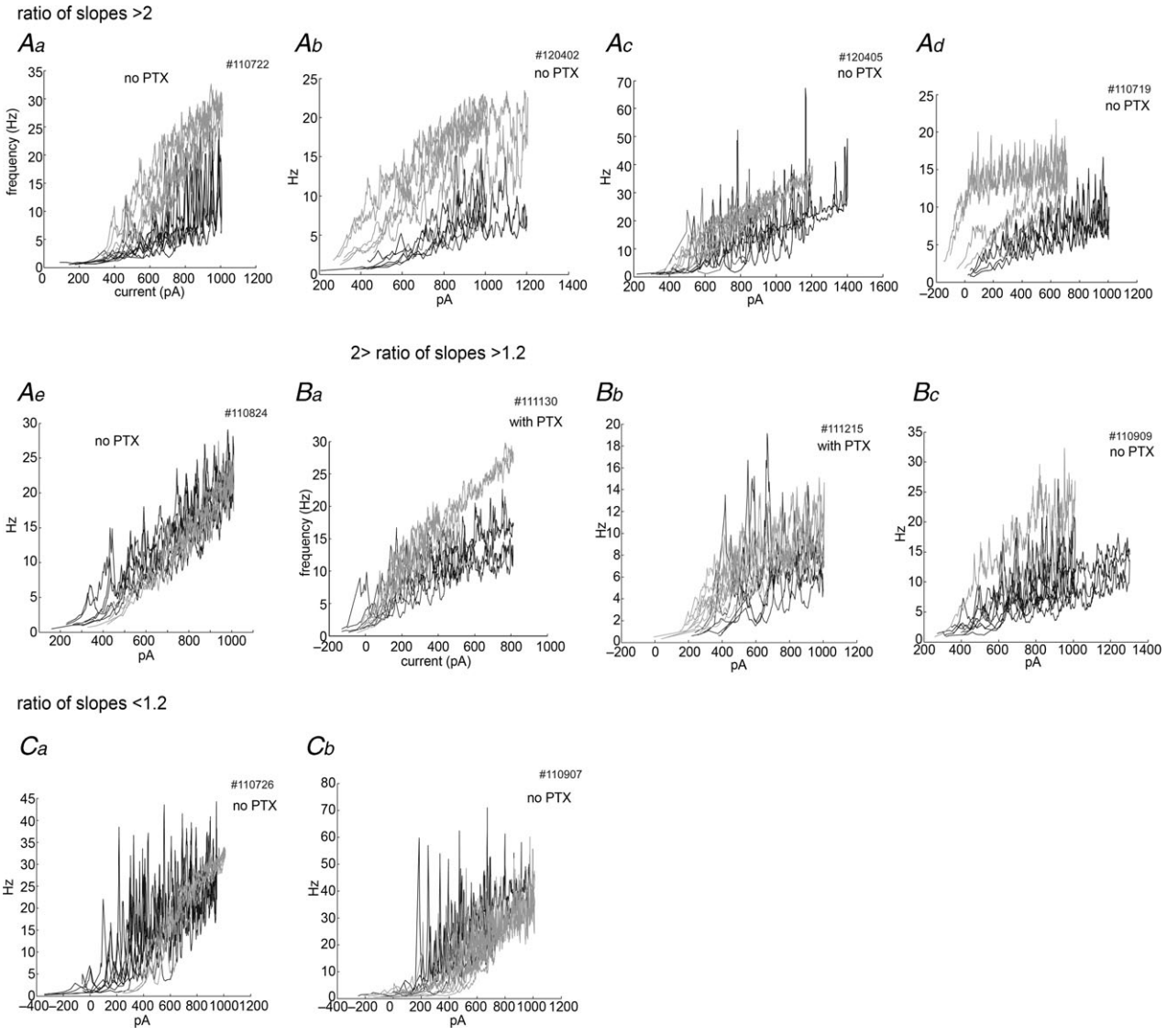

Figure 7. Most neurons show a steeper slope of the *f–I* curve during ramp stimulation after physostigmine application
Control traces (black) and physostigmine traces (grey) are overlaid for each cell. These data are aligned by the ratio of the averaged initial up-ramp slope in the presence of physostigmine to that in the control conditions. The ratio was larger than 2.0 in 5 neurons (*Aa–e*), between 1.2 and 2.0 in 3 neurons (*Ba–c*), and less than 1.2 in 2 neurons (*Ca–b*). Note that *Ad* and *Bc* showed clear hysteresis in the presence of physostigmine. Traces were smoothed by averaging 10 interspike intervals.

Table 1. All parameters of ramp stimulation data

Ramp no.	PTX	Ratio of slopes	Layer	Sag	R_{in} (Ctrl; MΩ)	R_{in} (Phys; MΩ)
110719	—	2.40	III	No	50	40
110722	—	8.30	II	Sag	7	9
110726	—	0.99	II	Sag	20	20
110824	—	2.10	II	Sag	34	34
110907	—	0.20	II	No	40	10
110909	—	1.13	II	Sag	14	25
111130	PTX	1.47	II	Sag	28	32
111215	PTX	1.34	II	Sag	22	23
120402	—	3.80	II	Sag	14	19
120405	—	2.47	III	Sag	35	40

Columns are as follows, from the left: the cell number; the use of picrotoxin (PTX) inside the recording pipette; the ratio of the averaged initial up-ramp slope in the presence of physostigmine to that in control conditions; layer; sag potential; and input resistance (R_{in}) in control conditions and after physostigmine (Phys).

However, the phenomenon of persistent spiking observed *in vitro* did not appear in our *in vivo* study, suggesting that intrinsic bistability of MEC neurons is not robust in the intact network and is not likely to correspond directly to delay activity underlying the storage of working memory. These results are a critical foundation for understanding the interactions of cellular properties of MEC neurons with network mechanisms of the functional medial temporal lobe circuit.

Decrease of resonance frequency by cholinergic modulation via h-current

The increase in cholinergic modulation induced by physostigmine administration in this experiment resulted in a decrease of sag amplitude, an increase of sag time constant and a decrease of resonance frequency *in vivo*, which is consistent with the data from *in vitro* slice preparations (Heys *et al.* 2010). The decrease of sag amplitude indicates a decrease of the I_h as shown in voltage-clamp studies *in vitro* (Heys & Hasselmo, 2012). The h-current (I_h) is a non-selective cation current, activated by hyperpolarization, meaning that it acts as a slow inward rectifier, mediated by HCN channels. Previous evidence suggests that the HCN channel has a critical role in resonance frequency (Nolan *et al.* 2004, 2007; Garden *et al.* 2008; Giocomo & Hasselmo, 2009), and differences in the composition of functional HCN channels by HCN1 and HCN2 subtypes appear to contribute to the dorsal–ventral gradient of resonance frequency in entorhinal neurons (Giocomo & Hasselmo, 2009). Knockout of the HCN1 subunit of the channel that mediates the h-current alters network theta rhythm amplitude (Nolan *et al.* 2004) and increases the size and spacing of the firing fields of grid cells in the MEC (Giocomo *et al.* 2011) and place cells in hippocampus (Hussaini *et al.* 2011). Given that I_h is the inductive element of resonance, the decrease of I_h exhibited by reduced sag can account for the decrease of resonance frequency with cholinergic modulation (Narayanan & Johnston, 2008). As the cholinergic system is active during arousal and attentional processes (Acquas *et al.* 1996; Parikh *et al.* 2007), the decrease of sag amplitude and decrease of resonance frequency might cause a change in the frequency of theta rhythm oscillations and thereby influence oscillatory interference (Hasselmo *et al.* 2007; Burgess, 2008; Hasselmo, 2008). These modulatory effects could underlie changes in the spacing of grid cells in novel environments (Barry *et al.* 2012*a*) and allow detection of a mismatch between grid cells with expanded spacing and other spatial inputs (Barry *et al.* 2012*b*).

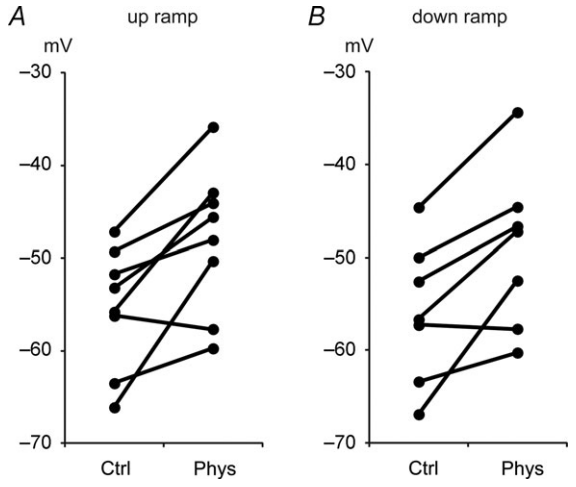

Figure 8. Spike thresholds are increased after physostigmine application
The thresholds of the first spike during up-ramp stimulation (*A*) and the thresholds of the last spike during down-ramp stimulation (*B*) before and after physostigmine application.

Absence of intrinsic bistable persistent spiking *in vivo*

Bistable persistent spiking and mechanistically related after-depolarizations or plateau potentials have been

reported throughout the extended medial temporal lobe memory system, including the MEC (Klink & Alonso, 1997*b*; Egorov *et al.* 2002), hippocampus (El-Hassar *et al.* 2011), subiculum (Kawasaki & Avoli, 1996; Kawasaki *et al.* 1999) and postsubiculum (Yoshida & Hasselmo, 2009). Seminal investigations of persistent spiking identified that the spiking state is dependent on a calcium-sensitive, non-selective cation current (I_{CAN}; Shalinsky *et al.* 2002; Fransén *et al.* 2006). Accumulating evidence now suggests that TRPC (transient receptor potential canonical) channels are responsible for the I_{CAN} that generates persistent spiking (Reboreda *et al.* 2011).

Perhaps the most dramatic difference between properties of neurons recorded *in vivo versus in vitro* was the absence of evidence for persistent spiking in our *in vivo* recordings, even though we used the same protocol which successfully induced persistent spiking *in vitro* (Egorov *et al.* 2002; Yoshida & Hasselmo, 2009; N. W. Schultheiss and M. E. Hasselmo, unpublished observations). We hypothesized that GABAergic input might prevent the appearance of persistent spiking. However, we did not observe persistent spiking in experiments with the $GABA_A$ receptor blocker, picrotoxin, in the pipette to cause selective blockade of inhibition on the recorded neuron, even though the firing frequency tended to be increased. One possible reason is that during *in vivo* recording, I_{CAN} might not be strong enough to elicit persistent spiking. Bistable persistent spiking depends on the balance between after-hyperpolarization (AHP) currents, which account for spike frequency adaptation (Vergara *et al.* 1998), and after-depolarization currents, which account for reverse spike frequency adaptation (Wilson *et al.* 2004). It is possible that the AHP effect is too strong to elicit bistable persistent spiking in the *in vivo* conditions. The SK channel, which mediates a medium or slow AHP current (I_{AHP}), is one of the candidates for inducing spike frequency adaptation (Vergara *et al.* 1998) in these neurons, but the slow I_{AHP} of stellate cells in MEC layer II is apamin insensitive (Khawaja *et al.* 2007). The apamin-insensitive SK channel might be the mediator to inhibit the bistable persistent spiking. Decrease of I_m (m-current), a slow voltage-sensitive K^+ current, by cholinergic input also depolarizes the membrane potential (Halliwell & Adams, 1982; Hu *et al.* 2002), but it was recently reported that I_m is not significantly present in stellate cells in layer II of the MEC (Heys & Hasselmo, 2012).

Another possible reason that persistent spiking might not appear *in vivo* is the relatively high membrane conductance compared with recordings *in vitro* (Fernandez & White, 2008). This high-conductance state might result in difficulties for neurons to maintain enough depolarization to induce persistent spiking.

Although we did not observe persistent spiking, in some cases a slight increase in firing was observed after the first depolarizing current injection, which might be the result of I_{CAN} activation. Although current injections to individual neurons can elicit persistent spiking with cholinergic modulation *in vitro*, we do not have evidence that persistent spiking occurs due to an intrinsic mechanism *in vivo*. This result indicates that some other mechanisms are needed to support persistent activity *in vivo*. Recently, Gupta *et al.* (2012) reported that persistent spiking was not observed during the delay period of a spatial delayed response task in awake, behaving rats. In previous studies, persistent spiking during the delay period was observed in EC (Suzuki *et al.* 1997; Young *et al.* 1997), but the population which showed persistent spiking was small. These reports suggest that the persistent spiking is much more rare *in vivo* than *in vitro*, and this is consistent with our finding.

There is a debate about whether persistent spiking occurs due to intrinsic mechanisms in single cells or network mechanisms involving interactions of multiple neurons. It might be possible that network input with multiple neurons is needed to maintain persistent spiking *in vivo*. Network mechanisms may contribute to the *in vivo* persistent spiking observed during sleep in layer III of medial entorhinal cortex (Hahn *et al.* 2012). It has also been reported that potassium conductances were increased by urethane in a visual cortex slice experiment (Sceniak & MacIver, 2006). It is possible that application of urethane diminishes the ability to elicit persistent spiking via the increase of potassium conductances.

In this study, most of the recorded cells were layer II neurons. Although persistent spiking is evident in some layer II neurons *in vitro* (N. W. Schultheiss and M. E. Hasselmo, personal communication), layer III and layer V neurons exhibit persistent spiking more reliably, perhaps contributing to the difficulty of observing persistent spiking in this study.

Further studies are needed to investigate whether and how intrinsic bistable persistent spiking can be elicited in the intact entorhinal network. They will help to understand the mechanism and meaning of the persistent neuronal activity *in vivo*.

Cholinergic modulation of the gain of spike frequency to input relationships

With cholinergic modulation, we observed that the initial slope of the measured *f–I* curves became considerably steeper in most cases than that in control conditions, and hysteresis was observed in several neurons. A steeper *f–I* curve indicates that neurons will change from a low-frequency firing state to a high-frequency firing state more rapidly with small increases in current application, which means that the sensitivity of the cell and the gain of the cell's input–output relationship are elevated. In cases where we observed hysteresis, firing frequency

increased steeply to a plateau during the up-ramp and then decreased during the down-ramp, resulting in an *f–I* plot that appears to transition in a clockwise manner during the ramp stimulus. The increased initial slope of the *f–I* relationship can be understood as a consequence of activation of I_{CAN}, which underlies persistent spiking *in vitro*, and reduced adaptation mediated by the decrease of K_{AHP} current. However, increased input resistance, which is probably mediated by blockade of leak current ($I_{K,leak}$; Cole & Nicoll, 1984) and/or inhibition of h-current observed during physostigmine administration, is likely also to contribute to the increase of the initial slope of the *f–I* curve. We did not observe any differences of ramp stimulation responses when comparing those experiments performed with picrotoxin *versus* those performed without picrotoxin application via the recording pipette. We noted the interesting observation that the spike threshold changes during cholinergic activation. This means that both the steeper *f–I* slope and the increase in spike threshold occur during cholinergic input. As a result, the cholinergic input makes a clearer contrast between the non-firing state and the firing state of the neuron. A possible mechanism for this threshold change is an influence of acetylcholine on the properties of voltage-dependent cation channels, including potassium channels and sodium channels (Klink & Alonso, 1997*b*). Another possibility is that modulation causes a difference in spike triggering sites, shifting from spike triggering near the soma to initiation of spikes in the dendrites at distal locations relative to the soma.

In summary, these results show that the cholinergic modulation of intrinsic resonance properties during *in vivo* intracellular recordings of MEC neurons are similar to data from *in vitro* recordings in brain slice preparations, but the recordings show differences in the cholinergic modulation of persistent spiking. These results provide insights concerning the modulation of intrinsic properties *in vivo*, and start to bridge the gap between the data from slice physiology and electrophysiological data from freely behaving animals. Further understanding of the effects of acetylcholine on intrinsic properties *in vivo* will help in understanding the role of acetylcholine in network theta rhythm oscillations and its role in behavioural mechanisms of attention and memory.

References

Acquas E, Wilson C & Fibiger HC (1996). Conditioned and unconditioned stimuli increase frontal cortical and hippocampal acetylcholine release: effects of novelty, habituation, and fear. *J Neurosci* **16**, 3089–3096.

Alonso A & Klink R (1993). Differential electroresponsiveness of stellate and pyramidal-like cells of medial entorhinal cortex layer II. *J Neurophysiol* **70**, 128–143.

Barry C, Ginzberg LL, O'Keefe J & Burgess N (2012*a*). Grid cell firing patterns signal environmental novelty by expansion. *Proc Natl Acad Sci U S A* **109**, 17687–17692.

Barry C, Heys JG & Hasselmo ME (2012*b*). Possible role of acetylcholine in regulating spatial novelty effects on theta rhythm and grid cells. *Front Neural Circuits* **6**, 1–13.

Brandon MP, Bogaard AR, Libby CP, Connerney MA, Gupta K & Hasselmo ME (2011). Reduction of theta rhythm dissociates grid cell spatial periodicity from directional tuning. *Science* **332**, 595–599.

Burgess N (2008). Grid cells and theta as oscillatory interference: theory and predictions. *Hippocampus* **18**, 1157–1174.

Button DC, Gardiner K, Marqueste T & Gardiner PF (2006). Frequency–current relationships of rat hindlimb α-motoneurones. *J Physiol* **573**, 663–677.

Camperi M & Wang XJ (1998). A model of visuospatial working memory in prefrontal cortex: recurrent network and cellular bistability. *J Comp Neurosci* **5**, 383–405.

Cole AE & Nicoll RA (1984). The pharmacology of cholinergic excitatory responses in hippocampal pyramidal cells. *Brain Res* **305**, 283–290.

Dickson CT, Magistretti J, Shalinsky MH, Fransén E, Hasselmo ME & Alonso A (2000). Properties and role of I_h in the pacing of subthreshold oscillations in entorhinal cortex layer II neurons. *J Neurophysiol* **83**, 2562–2579.

Dickson CT, Mena AR & Alonso A (1997). Electroresponsiveness of medial entorhinal cortex layer III neurons *in vitro*. *Neuroscience* **81**, 937–950.

Domnisoru C, Kinkhabwala AA & Tank DW (2013). Membrane potential dynamics of grid cells. *Nature* **495**, 199–204.

Egorov AV, Hamam BN, Fransén E, Hasselmo ME & Alonso AA (2002). Graded persistent activity in entorhinal cortex neurons. *Nature* **420**, 173–178.

El-Hassar L, Hagenston AM, D'Angelo LB & Yeckel MF (2011). Metabotropic glutamate receptors regulate hippocampal CA1 pyramidal neuron excitability via Ca^{2+} wave-dependent activation of SK and TRPC channels. *J Physiol* **589**, 3211–3229.

Erchova I, Kreck G, Heinemann U & Herz AVM (2004). Dynamics of rat entorhinal cortex layer II and III cells: characteristics of membrane potential resonance at rest predict oscillation properties near threshold. *J Physiol* **560**, 89–110.

Fernandez FR & White JA (2008). Artificial synaptic conductances reduce subthreshold oscillations and periodic firing in stellate cells of the entorhinal cortex. *J Neurosci* **28**, 3790–3803.

Fransén E, Tahvildari B, Egorov AV, Hasselmo ME & Alonso AA (2006). Mechanism of graded persistent cellular activity of entorhinal cortex layer V neurons. *Neuron* **49**, 735–746.

Garden DLF, Dodson PD, O'Donnell C, White MD & Nolan MF (2008). Tuning of synaptic integration in the medial entorhinal cortex to the organization of grid cell firing fields. *Neuron* **60**, 875–889.

Giocomo LM & Hasselmo ME (2008). Time constants of h current in layer II stellate cells differ along the dorsal to ventral axis of medial entorhinal cortex. *J Neurosci* **28**, 9414–9425.

Giocomo LM & Hasselmo ME (2009). Knock-out of HCN1 subunit flattens dorsal–ventral frequency gradient of medial entorhinal neurons in adult mice. *J Neurosci* **29**, 7625–7630.

Giocomo LM, Hussaini SA, Zheng F, Kandel ER, Moser M-B & Moser EI (2011). Grid cells use HCN1 channels for spatial scaling. *Cell* **147**, 1159–1170.

Giocomo LM, Zilli EA, Fransén E & Hasselmo ME (2007). Temporal frequency of subthreshold oscillations scales with entorhinal grid cell field spacing. *Science* **315**, 1719–1722.

Gloveli T, Schmitz D, Empson RM, Dugladze T & Heinemann U (1997). Morphological and electrophysiological characterization of layer III cells of the medial entorhinal cortex of the rat. *Neuroscience* **77**, 629–648.

Gupta K, Keller LA & Hasselmo ME (2012). Reduced spiking in entorhinal cortex during the delay period of a cued spatial response task. *Learn Mem* **19**, 219–230.

Hafting T, Fyhn M, Molden S, Moser M-B & Moser EI (2005). Microstructure of a spatial map in the entorhinal cortex. *Nature* **436**, 801–806.

Hahn TTG, McFarland JM, Berberich S, Sakmann B & Mehta MR (2012). Spontaneous persistent activity in entorhinal cortex modulates cortico-hippocampal interaction in vivo. *Nat Neurosci* **15**, 1531–1538.

Halliwell JV & Adams PR (1982). Voltage-clamp analysis of muscarinic excitation in hippocampal neurons. *Brain Res* **250**, 71–92.

Hasselmo ME (2006). The role of acetylcholine in learning and memory. *Curr Opin Neurobiol* **16**, 710–715.

Hasselmo ME (2008). Grid cell mechanisms and function: contributions of entorhinal persistent spiking and phase resetting. *Hippocampus* **18**, 1213–1229.

Hasselmo ME, Giocomo LM & Zilli EA (2007). Grid cell firing may arise from interference of theta frequency membrane potential oscillations in single neurons. *Hippocampus* **17**, 1252–1271.

Hasselmo ME & Stern CE (2006). Mechanisms underlying working memory for novel information. *Trends Cogn Sci* **10**, 487–493.

Heys JG, Giocomo LM & Hasselmo ME (2010). Cholinergic modulation of the resonance properties of stellate cells in layer II of medial entorhinal cortex. *J Neurophysiol* **104**, 258–270.

Heys JG & Hasselmo ME (2012). Neuromodulation of I_h in layer II medial entorhinal cortex stellate cells: a voltage-clamp study. *J Neurosci* **32**, 9066–9072.

Heys JG, Schultheiss NW, Shay CF, Tsuno Y & Hasselmo ME (2012). Effects of acetylcholine on neuronal properties in entorhinal cortex. *Front Behav Neurosci* **6**, 32.

Hu H, Vervaeke K, Graham LJ & Storm JF (2009). Complementary theta resonance filtering by two spatially segregated mechanisms in CA1 hippocampal pyramidal neurons. *J Neurosci* **29**, 14472–14483.

Hu H, Vervaeke K & Storm JF (2002). Two forms of electrical resonance at theta frequencies, generated by M-current, h-current and persistent Na^+ current in rat hippocampal pyramidal cells. *J Physiol* **545**, 783–805.

Hussaini SA, Kempadoo KA, Thuault SJ, Siegelbaum SA & Kandel ER (2011). Increased size and stability of CA1 and CA3 place fields in HCN1 knockout mice. *Neuron* **72**, 643–653.

Hutcheon B & Yarom Y (2000). Resonance, oscillation and the intrinsic frequency preferences of neurons. *Trends Neurosci* **23**, 216–222.

Iglesias C, Meunier C, Manuel M, Timofeeva Y, Delestrée N & Zytnicki D (2011). Mixed mode oscillations in mouse spinal motoneurons arise from a low excitability state. *J Neurosci* **31**, 5829–5840.

Kawasaki H & Avoli M (1996). Excitatory effects induced by carbachol on bursting neurons of the rat subiculum. *Neurosci Lett* **219**, 1–4.

Kawasaki H, Palmieri C & Avoli M (1999). Muscarinic receptor activation induces depolarizing plateau potentials in bursting neurons of the rat subiculum. *J Neurophysiol* **82**, 2590–2601.

Khawaja FA, Alonso AA & Bourque CW (2007). Ca^{2+}-dependent K^+ currents and spike-frequency adaptation in medial entorhinal cortex layer II stellate cells. *Hippocampus* **17**, 1143–1148.

Klink R & Alonso A (1997*a*). Morphological characteristics of layer II projection neurons in the rat medial entorhinal cortex. *Hippocampus* **7**, 571–583.

Klink R & Alonso A (1997*b*). Muscarinic modulation of the oscillatory and repetitive firing properties of entorhinal cortex layer II neurons. *J Neurophysiol* **77**, 1813–1828.

Koenig J, Linder AN, Leutgeb JK & Leutgeb S (2011). The spatial periodicity of grid cells is not sustained during reduced theta oscillations. *Science* **332**, 592–595.

Leonard BW, Amaral DG, Squire LR & Zola-Morgan S (1995). Transient memory impairment in monkeys with bilateral lesions of the entorhinal cortex. *J Neurosci* **15**, 5637–5659.

Ludwig A, Zong X, Jeglitsch M, Hofmann F & Biel M (1998). A family of hyperpolarization-activated mammalian cation channels. *Nature* **393**, 587–591.

Major G & Tank D (2004). Persistent neural activity: prevalence and mechanisms. *Curr Opin Neurobiol* **14**, 675–684.

Manns ID, Alonso A & Jones BE (2000). Discharge properties of juxtacellularly labeled and immunohistochemically identified cholinergic basal forebrain neurons recorded in association with the electroencephalogram in anesthetized rats. *J Neurosci* **20**, 1505–1518.

Moser EI & Moser M-B (2008). A metric for space. *Hippocampus* **18**, 1142–1156.

Murakami M, Kashiwadani H, Kirino Y & Mori K (2005). State-dependent sensory gating in olfactory cortex. *Neuron* **46**, 285–296.

Narayanan R & Johnston D (2008). The h channel mediates location dependence and plasticity of intrinsic phase response in rat hippocampal neurons. *J Neurosci* **28**, 5846–5860.

Newman EL, Gupta K, Climer JR, Monaghan CK & Hasselmo ME (2012). Cholinergic modulation of cognitive processing: insights drawn from computational models. *Front Behav Neurosci* **6**, 24.

Nolan MF, Dudman JT, Dodson PD & Santoro B (2007). HCN1 channels control resting and active integrative properties of stellate cells from layer II of the entorhinal cortex. *J Neurosci* **27**, 12440–12451.

Nolan MF, Malleret G, Dudman JT, Buhl DL, Santoro B, Gibbs E, Vronskaya S, Buzsáki G, Siegelbaum SA, Kandel ER & Morozov A (2004). A behavioral role for dendritic integration: HCN1 channels constrain spatial memory and plasticity at inputs to distal dendrites of CA1 pyramidal neurons. *Cell* **119**, 719–732.

Parikh V, Kozak R, Martinez V & Sarter M (2007). Prefrontal acetylcholine release controls cue detection on multiple timescales. *Neuron* **56**, 141–154.

Quilichini P, Sirota A & Buzsáki G (2010). Intrinsic circuit organization and theta–gamma oscillation dynamics in the entorhinal cortex of the rat. *J Neurosci* **30**, 11128–11142.

Reboreda A, Jiménez-Díaz L & Navarro-López JD (2011). TRP channels and neural persistent activity. *Adv Exp Med Biol* **704**, 595–613.

Sceniak MP & MacIver MB (2006). Cellular actions of urethane on rat visual cortical neurons in vitro. *J Neurophysiol* **95**, 3865–3874.

Schall KP & Dickson CT (2010). Changes in hippocampal excitatory synaptic transmission during cholinergically induced theta and slow oscillation states. *Hippocampus* **20**, 279–292.

Schmidt-Hieber C & Häusser M (2013). Cellular mechanisms of spatial navigation in the medial entorhinal cortex. *Nat Neurosci* **16**, 325–331.

Schon K, Atri A, Hasselmo ME, Tricarico MD, LoPresti ML & Stern CE (2005). Scopolamine reduces persistent activity related to long-term encoding in the parahippocampal gyrus during delayed matching in humans. *J Neurosci* **25**, 9112–9123.

Schon K, Hasselmo ME, Lopresti ML, Tricarico MD & Stern CE (2004). Persistence of parahippocampal representation in the absence of stimulus input enhances long-term encoding: a functional magnetic resonance imaging study of subsequent memory after a delayed match-to-sample task. *J Neurosci* **24**, 11088–11097.

Schultheiss NW & Hasselmo ME (2011). Persistent spiking of medial entorhinal cortical neurons during theta frequency oscillations in vitro. Program No. 730.11. 2011 Neuroscience Meeting Planner. Washington, DC: Society for Neuroscience, 2011. Online http://www.abstractsonline.com/Plan/ViewAbstract.aspx?sKey=b55b2d4a-c543-4ce7-8061-31814b571874&cKey=0c87867e-4912-4b6f-a387-0311cec0af97&mKey=%7b8334BE29-8911-4991-8C31-32B32DD5E6C8%7d Last accessed on April 9, 2013.

Shalinsky MH, Magistretti J, Ma L & Alonso AA (2002). Muscarinic activation of a cation current and associated current noise in entorhinal-cortex layer-II neurons. *J Neurophysiol* **88**, 1197–1211.

Steffenach HA, Witter M, Moser MB & Moser EI (2005). Spatial memory in the rat requires the dorsolateral band of the entorhinal cortex. *Neuron* **45**, 301–13.

Suzuki WA, Miller EK & Desimone R (1997). Object and place memory in the macaque entorhinal cortex. *J Neurophysiol* **78**, 1062–1081.

Tahvildari B, Fransén E, Alonso AA & Hasselmo ME (2007). Switching between "On" and "Off" states of persistent activity in lateral entorhinal layer III neurons. *Hippocampus* **17**, 257–263.

Tsuno Y, Kashiwadani H & Mori K (2008). Behavioral state regulation of dendrodendritic synaptic inhibition in the olfactory bulb. *J Neurosci* **28**, 9227–9238.

van Strien NM, Cappaert NLM & Witter MP (2009). The anatomy of memory: an interactive overview of the parahippocampal–hippocampal network. *Nat Rev Neurosci* **10**, 272–282.

Vergara C, Latorre R, Marrion NV & Adelman JP (1998). Calcium-activated potassium channels. *Curr Opin Neurobiol* **8**, 321–329.

Wilson CJ, Weyrick A, Terman D, Hallworth NE & Bevan MD (2004). A model of reverse spike frequency adaptation and repetitive firing of subthalamic nucleus neurons. *J Neurophysiol* **91**, 1963–1980.

Witter MP, Groenewegen HJ, Lopes da Silva FH & Lohman AH (1989). Functional organization of the extrinsic and intrinsic circuitry of the parahippocampal region. *Prog Neurobiol* **33**, 161–253.

Wolansky T, Clement EA, Peters SR, Palczak MA & Dickson CT (2006). Hippocampal slow oscillation: a novel EEG state and its coordination with ongoing neocortical activity. *J Neurosci* **26**, 6213–6229.

Yazaki-Sugiyama Y, Kang S, Câteau H, Fukai T & Hensch TK (2009). Bidirectional plasticity in fast-spiking GABA circuits by visual experience. *Nature* **462**, 218–221.

Yoshida M & Hasselmo ME (2009). Persistent firing supported by an intrinsic cellular mechanism in a component of the head direction system. *J Neurosci* **29**, 4945–4952.

Young BJ, Otto T, Fox GD & Eichenbaum H (1997). Memory representation within the parahippocampal region. *J Neurosci* **17**, 5183–5195.

Zhang Z, Reboreda A, Alonso A, Barker PA & Séguéla P (2011). TRPC channels underlie cholinergic plateau potentials and persistent activity in entorhinal cortex. *Hippocampus* **21**, 386–397.

Author contributions

Y.T., N.W.S. and M.E.H. designed the experiments, interpreted data and wrote the article. Y.T. collected all data. Y.T. and N.W.S. performed analysis. All the authors approved the final version for publication.

Acknowledgements

This work was supported by National Institute of Mental Health (NIMH) R01 grants MH61492, MH60013 and ONR MURI N00014-10-1-0936. This work was also supported by the Uehara memorial foundation (Y.T.). We would like to thank Dr James G. Heys, Dr Motoharu Yoshida, Dr Ehren Newman, Dr Erik Fransén, Tyler Ware, Jason Climer, Dr Eric Zilli and all Hasselmo laboratory members for useful comments. We also thank Professor Matt Wachowiak for assistance with the experimental set-up and Professors Chantal E. Stern and Howard Eichenbaum for the use of laboratory resources.